CRISPR

# Structural basis for RNA-guided DNA cleavage by IscB-ωRNA and mechanistic comparison with Cas9

Gabriel Schuler†, Chunyi Hu†, Ailong Ke*

Class 2 CRISPR effectors Cas9 and Cas12 may have evolved from nucleases in IS200/IS605 transposons. IscB is about two-fifths the size of Cas9 but shares a similar domain organization. The associated ωRNA plays the combined role of CRISPR RNA (crRNA) and trans-activating CRISPR RNA (tracrRNA) to guide double-stranded DNA (dsDNA) cleavage. Here we report a 2.78-angstrom cryo–electron microscopy structure of IscB-ωRNA bound to a dsDNA target, revealing the architectural and mechanistic similarities between IscB and Cas9 ribonucleoproteins. Target-adjacent motif recognition, R-loop formation, and DNA cleavage mechanisms are explained at high resolution. ωRNA plays the equivalent function of REC domains in Cas9 and contacts the RNA-DNA heteroduplex. The IscB-specific PLMP domain is dispensable for RNA-guided DNA cleavage. The transition from ancestral IscB to Cas9 involved dwarfing the ωRNA and introducing protein domain replacements.

Increasing evidence points to the possibility that the core components of the CRISPR-Cas adaptive immune systems evolved from genes in mobile genetic elements. The class 2 CRISPR effectors Cas9 (type II) and Cas12 (type V) are believed to have independently evolved from an ancestral TnpB-like nuclease, which is still commonly found in insertion sequence (IS) elements today (*1*–*3*). Cas9 appears to have emerged from a distinct branch of IS elements within the IS200/IS605 superfamily harboring IscB (*2*). IscB and Cas9 share a common domain architecture at the sequence level (Fig. 1, A and B). Both contain an arginine-rich bridge helix and an HNH endonuclease domain inserted into a RuvC endonuclease domain (*1*, *2*). The bridge helix in Cas9 plays a crucial role in mediating complex ribonucleoprotein (RNP) formation with two noncoding RNAs, CRISPR RNA (crRNA) and trans-activating CRISPR RNA (tracrRNA) (*4*–*8*). HNH and RuvC endonucleases are used by Cas9 to cleave the target and nontarget DNA strands, respectively (*4*). During CRISPR interference, the DNA substrate is validated through R-loop formation, which involves DNA unwinding and RNA-DNA heteroduplex formation (*7*, *9*–*14*). IscB was found to assemble with a single large [>200 nucleotides (nt)] noncoding RNA encoded by the transposon, ωRNA (OMEGA: obligate mobile element guided activity) (*2*). Together IscB-ωRNA mediates RNA-guided DNA cleavage similar to the Cas9-crRNA-tracrRNA RNP (*2*). To avoid self-targeting and to reduce search space, Cas9 further specifies a protospacer adjacent motif (PAM) adjacent to the target site (*15*, *16*). This mechanism is conserved in IscB-ωRNA, and the equivalent target-adjacent motif (TAM) is recognized by a TAM interaction domain (TID) in IscB (*2*). All IscBs further encode a PLMP-motif containing domain at the N terminus (*2*). This domain is not found in Cas9 and has an undefined function (Fig. 1B).

To understand the RNA-guided DNA cleavage mechanism by the compact IscB-ωRNA RNP and its relationship with Cas9-crRNA-tracrRNA, we determined a 2.78-Å structure of the gut microbiome–derived *Ogeu*IscB-ωRNA RNP complex (*2*) bound to target DNA using cryo–electron microscopy (cryo-EM) (Fig. 1, figs. S1 to S3, and movie S1). Whereas the majority of the 496–amino acid IscB and 222-nt ωRNA could be unambiguously resolved, only a portion of the 60–base pair (bp) DNA target could be reliably modeled. These include 13 bp of the TAM-proximal double-stranded DNA (dsDNA), the entire 16-nt target strand (TS) single-stranded DNA (ssDNA), and the 2-nt nontarget strand (NTS) ssDNA in the R-loop region (Fig. 2A). The TAM-distal DNA is missing from the EM density owing to molecular motion rather than cleavage and dissociation, because phosphorothioate modifications have been introduced into the DNA backbone at the HNH and RuvC cleavage sites (fig. S1H) (*2*).

We found that the architectural organization, domain functionality, and nucleic acid binding mode are similar between IscB-ωRNA and Cas9 RNP. IscB-ωRNA adopts a similar two-lobed architecture, although its overall shape is much flatter, because several surface

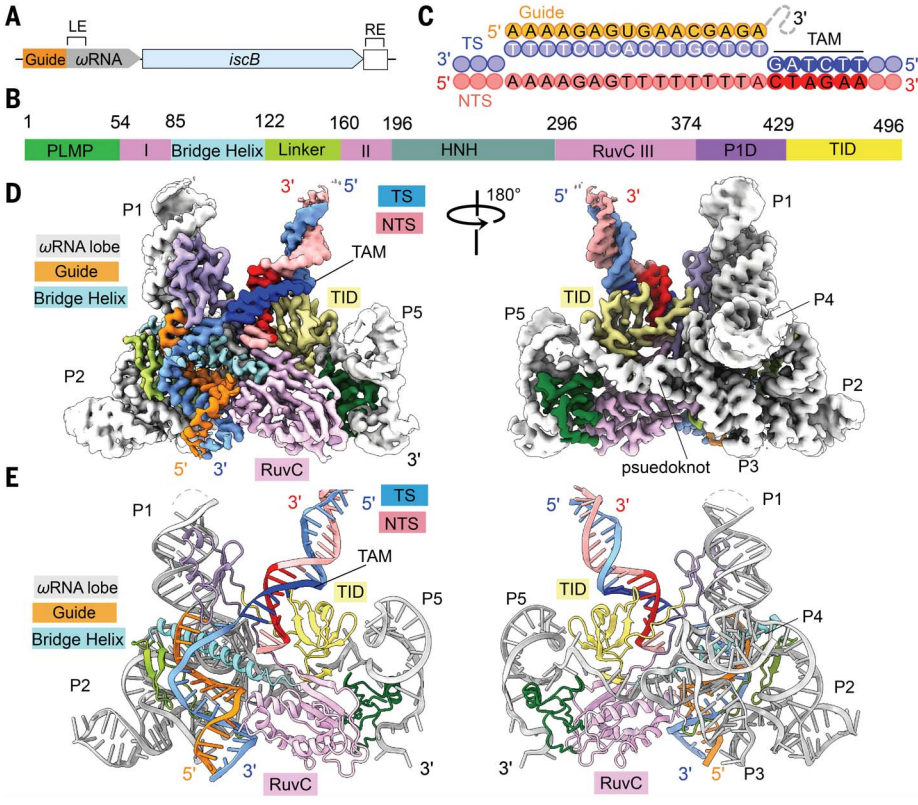


**Fig. 1. Cryo-EM reconstruction and structure of IscB RNP bound to target DNA.** (**A**) Arrangement of the *Ogeu*IscB and ωRNA in its native IS element defined by the left (LE) and right (RE) ends of the transposon. (**B**) Domain organization of IscB. P1D, P1 interaction domain; TID, TAM-interaction domain. RuvC domain is separated into three segments: RuvC I, II, and III. Color scheme is conserved throughout Fig. 1. (**C**) Diagram of R-loop formed between guide RNA and target DNA. TAM sequence is read 5′-CTAGAA-3′ on the nontarget strand. (**D** and **E**) Cryo-EM reconstruction at 2.78 Å and cartoon representations of the IscB-ωRNA/target DNA complex.

Department of Molecular Biology and Genetics, Cornell University, 253 Biotechnology Building, Ithaca, NY 14853, USA.
*Corresponding author. Email: ailong.ke@cornell.edu
†These authors contributed equally to this work.

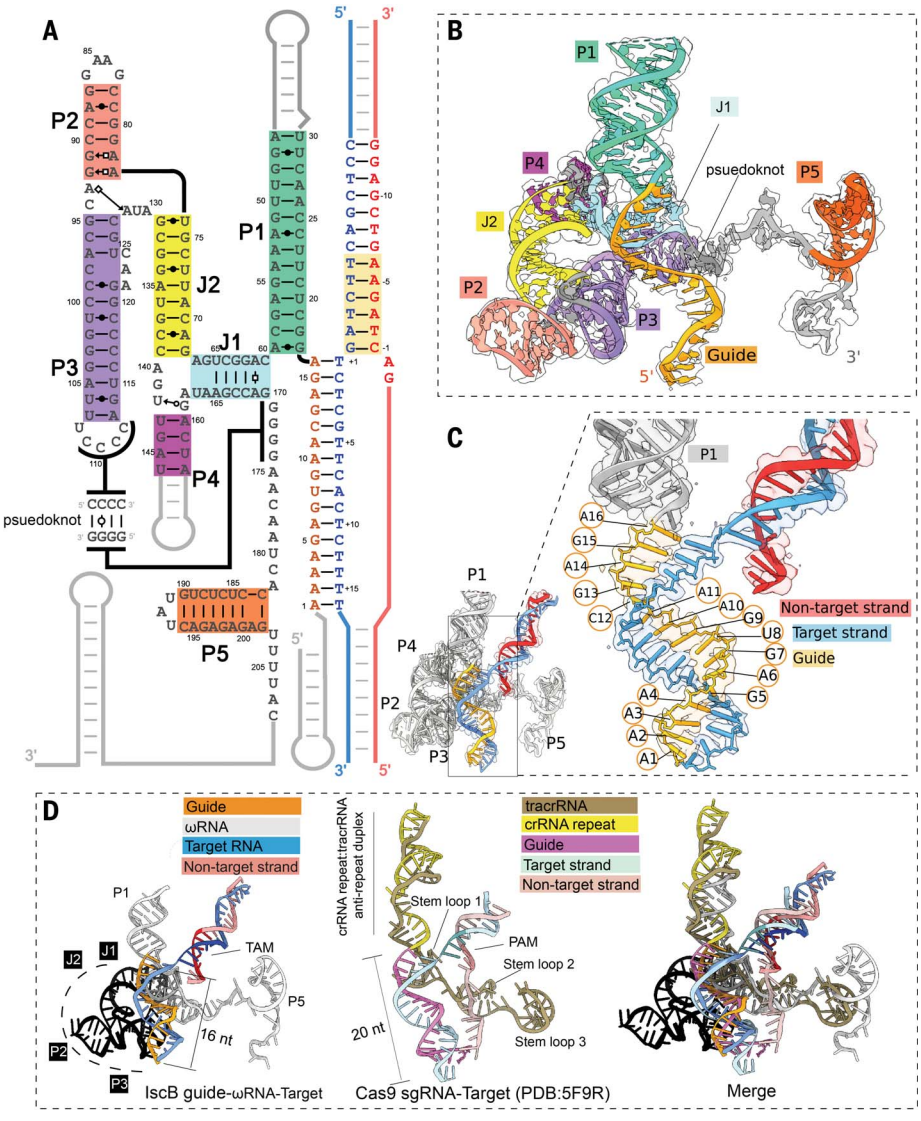


**Fig. 2. Structural organization of the ωRNA and comparison to Cas9 crRNA-tracrRNA.** (**A**) Schematic of ωRNA depicting secondary and tertiary interactions. Nontarget strand, red; target strand, blue; guide RNA, orange. (**B**) Atomic model of ωRNA. (**C**) Close-up view depicting R-loop base pairing between guide RNA and target strand DNA. (**D**) Structural alignment of ωRNA and tracrRNA-crRNA in *Sp*Cas9 RNP showing conserved RNA structures in guide RNAs, P1 with *Sp*Cas9 tracrRNA-crRNA helix, J1 with *Sp*Cas9 tracrRNA stem loop 1, P3 pseudoknot with *Sp*Cas9 tracrRNA stem loop 2, and P5 with *Sp*Cas9 tracrRNA stem loop 3. Colored in black is the region of the ωRNA replaced by the REC lobe in Cas9.

domains in Cas9 are missing in IscB (fig. S4 and movie S2). Structural alignments revealed that the P1 stem loop of ωRNA is the functional equivalent of the crRNA repeat–tracrRNA anti-repeat duplex in the Cas9 RNP. It occupies the same location in the RNP and assists R-loop formation in a similar manner, by stabilizing the guide-RNA/TS-DNA heteroduplex through continuous base stacking (Fig. 1, C to E, and movie S3). The TAM-containing dsDNA and the guide-RNA/TS-DNA heteroduplex in the R-loop region are accommodated by IscB-ωRNA at locations similar to those in Cas9s, through conceptually similar mechanisms (Fig. 1, D and E, and fig. S4). The TS-DNA base-pairs with the 16-nt guide RNA. The first 12 bp of the DNA-RNA heteroduplex adopts a distorted A-form owing to IscB contacts, with a widened major groove and base-stacking almost perpendicular to the helical axis. The last 4 bp of the heteroduplex adopts a canonical A-form geometry (Fig. 1, D and E).

Architecturally, the biggest structural difference between IscB and Cas9 is its lack of a polypeptide-based recognition (REC) lobe (fig. S4 and movie S2). The functional replacement is the ωRNA lobe (from J1 to the pseudoknot), which folds into a sophisticated tertiary RNA structure (Fig. 2A). The structured portion of ωRNA was previously identified as HEARO RNA [HNH endonuclease–associated RNA and ORF (open reading frame)] (*17*). This RNA and its associated HNH-containing ORF together were speculated to constitute a mobile genetic element (*17*). The three-dimensional (3D) structure supports the secondary structure models from previous studies (*2*, *17*). The central portion of ωRNA is a tail-to-tail stacked P2-P3 superhelix. J2 helix extrudes from the P2-P3 junction, then bifurcates into P4 and J1 at its end. Whereas P4 projects away, J1 projects toward the apex of P3. The following residues zip up with the apical loop of P3 through a 4-bp G/C-rich pseudoknot (Fig. 2, A and B). Following the pseudoknot, ωRNA extends horizontally along the back side of the IscB as a conserved single-stranded linker and a terminator-like element (P5, followed by four consecutive U's) (Fig. 2B). A conserved and highly structured RNA typically mediates either catalysis, ligand binding, or RNP formation (*17*). Our structure does not support a direct involvement of ωRNA in RNA-guided DNA cleavage because the bulk of ωRNA is insulated from the guide-RNA/TS-DNA heteroduplex by a layer of protein elements from IscB (Figs. 1, C and D, and 2C and movie S1). Our structure further suggests that the evolutionary trend from ancestral IscB to Cas9 involves replacing the structural roles of ωRNA with protein domains. However, the crRNA-tracrRNA of SpCas9 and NmeCas9 RNPs still contain structural elements reminiscent of P1, J1, pseudoknot, and terminator in ωRNA (Fig. 2D and fig. S5), presumably because these elements are indispensable for RNP assembly.

Opposite from the ωRNA lobe, the equivalent of the Cas9 nuclease (NUC) lobe contains the RuvC nuclease as its platform. RuvC is woven together from three split polypeptide elements (Fig. 1B, fig. S6A, and movie S1). It projects structural domains to various regions of the RNP. These elements are rich in positive surface charges, making favorable contacts with nucleic acids in different regions (fig. S6A). The N-terminal PLMP motif–containing domain is packed at the edge of the NUC lobe to capture the terminator-like structure in ωRNA (fig. S6B). The Arg-rich bridge helix is regarded as one of the most conserved structural elements in Cas9 (*7*, *8*). It plays an equally important function in IscB-ωRNA RNP. Projected from RuvC, the bridge helix travels underneath the guide RNA, along the pseudoknot and J1, and at the base of P1, making multiple electrostatic contacts to the sugar-phosphate backbones. A line of consecutive arginine and lysine residues along one phase of the bridge helix make consecutive phosphate contacts to seven residues in the RNA guide (U8-A14), immobilizing the seed region of the guide in place for TS-DNA base

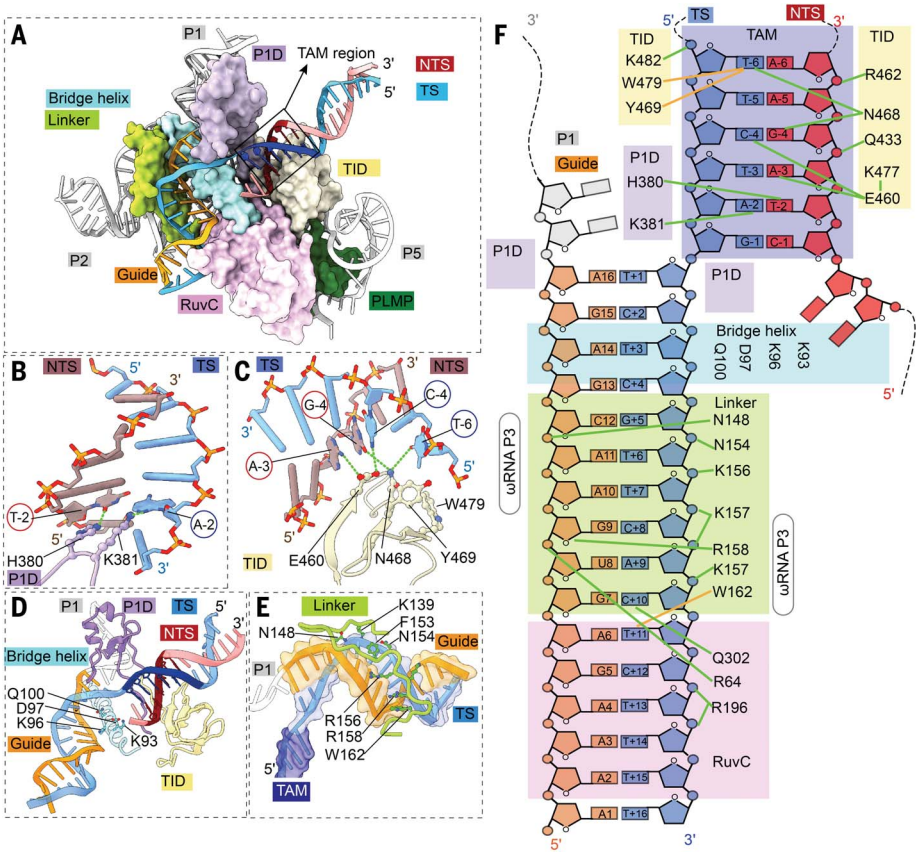


**Fig. 3. Structural basis for TAM recognition and R-loop formation by IscB-ωRNA.** (**A**) TAM recognition and R-loop specification by domains of IscB. Color scheme is consistent with that in Fig. 1. (**B**) Close-up view of P1 interaction domain (P1D) linker residues recognizing TAM-2 base pair (target adjacent motif) from the DNA minor groove side. (**C**) Close-up view of the IscB TAM interaction domain (TID) making base-specific contacts from the DNA major groove side. (**D**) Close-up view of the bridge helix and P1D making contacts with the beginning portion of the DNA-RNA heteroduplex in the R-loop region. (**E**) Close-up view of the β hairpin+linker domain specifying the minor groove of the middle portion of the DNA-RNA heteroduplex. (**F**) Diagram of IscB contacts to TAM and DNA-RNA heteroduplex in the R-loop. Positioning of the bridge helix domain separating the R-loop from the core of ωRNA in light blue. Green lines denote electrostatic contacts and brown lines denote hydrophobic contacts. TAM highlighted with purple box (ideal TAM sequence: 5′-NWRRNA-3′). guide RNA (orange), target strand DNA (blue), nontarget strand DNA (red).

pairing (fig. S6C). A β hairpin followed by a flexible linker connects the bridge helix back to RuvC. Although very degenerate in size and structural complexity, this flexible structural elements "glues" ωRNA and middle portion of the guide RNA together with its positive Arg and Lys residues (fig. S6D). The HNH nuclease domain is projected internally from RuvC. As in many Cas9s, this domain is not well resolved in the averaged EM density map owing to conformational flexibility. RuvC sends P1D domain to recognize the P1 helix of ωRNA; its functional equivalence is the WED domain in Cas9 (figs. S6E and S4) (*7*, *10*, *16*). Finally, P1D connects with the TAM-interaction domain (TID) situated above RuvC through flexible linkers.

The *Ogeu*IscB-ωRNA/R-loop structure explains the RNA-guided target recognition mechanism in high resolution (Fig. 3A and movie S4). TAM [5′-NWRRNA-3′ (*2*); actual sequence: CTAGAA] in the dsDNA target is captured from the major groove side by the TID domain of IscB and from the minor groove side by the P1D linker (Figs. 3B and 4, C and F). No contact was found at the −1 TAM position. The −2 TAM position is recognized from the minor groove side by His$^{397}$ and Lys$^{380}$ in P1D linker to O2 of $T_{NTS-2}$ and N3 of $A_{TS-2}$, respectively. G-C pairs may be rejected in either combination owing to the steric clash caused by the N2 protrusion from guanosine into the minor groove. The −3 and −4 of TAM appear to be probed indirectly for shape complementarity. It is likely that only purines in the NTS support the van der Waals contacts to the backbone of Glu$^{459}$ and Gly$^{460}$ in TID; pyrimidines are too recessed. The −6 TAM position is recognized through hydrophobic contacts to the methyl groups of $T_{TS-6}$ in the major grove, by Tyr$^{468}$ and Trp$^{478}$ in TID, respectively. Many IscB homologs encode smaller TID domains and specify less stringent TAM codes (*2*). Domain-swapping attempts, structure-guided design, and directed evolution could lead to more versatile IscB-ωRNA tools with expanded TAM codes.

A recent Cas9 study showed that off-targeting is inversely correlated with the extent of protein contacts to the guide-RNA/TS-DNA heteroduplex; the more local interactions to specify an A-form geometry, the less mismatch tolerance therein (*14*). In this regard, our structural analysis identified extensive R-loop contacts (Figs. 3A and 4, D to F), which implies that IscB-ωRNA can specify a DNA target stringently despite its miniature size and shorter R-loop specification. A P1D loop (amino acids 396 to 408) specifies the first two base pairs of the guide-RNA/TS-DNA heteroduplex from the minor groove side. The bridge helix and the following β hairpin and linker specify the middle portion of the heteroduplex (bp 2 to 9) from major and minor sides, respectively. ωRNA provides the platform support for these contacts, and a portion of the ωRNA backbone (P2, nt 114 to 116) directly contacts the backbone of guide RNA (bp 10 and 11). The RuvC domain then contacts the minor groove of bp 9 to 13. Base pairs 14 to 16 are not contacted and have weaker density. As shown later, this region is recognized when HNH docks onto the DNA-RNA heteroduplex.

To gain insight into the DNA cleavage mechanism, we analyzed the conformational dynamics in the IscB-ωRNA/R-loop EM reconstruction. Finer conformational sampling revealed two predominant conformational states. In the unlocked R-loop state (Fig. 4, A and B, and fig. S7), the 3.1-Å map shows the NTS-DNA traveling near the RNA-bound TS-DNA. NTS-DNA is blocked from accessing the RuvC active site because of a steric clash with the anchor connecting HNH to RuvC (Fig. 4A). Although unresolved in EM density, HNH is likely part of the blocking mechanism as well. Its approximate location can be inferred by comparing it to the NmeCas9 *apo* structure (*12*). By contrast, the 3.2-Å locked R-loop state (Fig. 4, C and D) shows HNH docking onto the RNA/TS-DNA heteroduplex and caging it with the rest of the IscB elements mentioned previously (Figs. 3A and 4C and movie S5). The entry and exiting linkers from RuvC to HNH probe for shape complementarity with the bottom and middle portions of the DNA-RNA heteroduplex, respectively. The body of HNH sinks into the major groove of the DNA-RNA heteroduplex (Fig. 4C). These close contacts are expected to further reduce mismatch tolerance. An Alphafold (*18*) predicted HNH

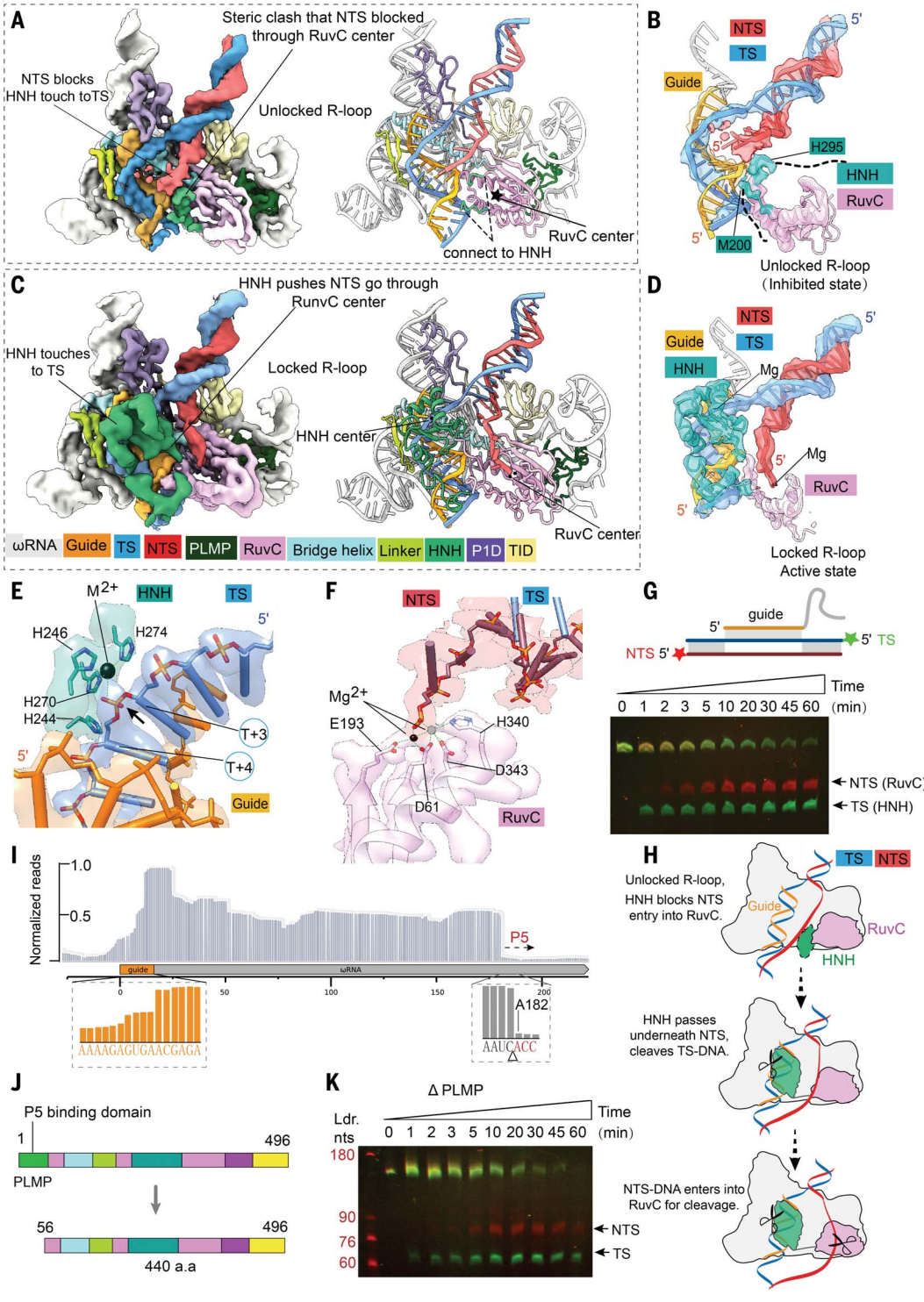


**Fig. 4. Mechanistic dissection of RNA-guided DNA cleavage by IscB.** (**A**) A 3.7-Å EM map and atomic model depicting the unlocked R-loop state. Color scheme is consistent with that in Fig. 1. (**B**) Focused view of DNA, guide RNA, and nuclease densities seen in the unlocked R-loop state. NTS is blocked from entering the RuvC cleavage site by the anchor of HNH to RuvC. (**C**) A 3.8-Å EM map and atomic model of the locked R-loop state. Alphafold predicted HNH domain structure (in green) is docked unambiguously into the EM density. Linker between HNH and RuvC domains can be seen interacting with the TAM-distal portion of the R-loop. (**D**) Focused view of HNH densities in the locked (active) state. The NTS density is now allowed into the RuvC active site. (**E**) Close-up view of the HNH active site in the locked state. Catalytic metal ion (black) is seen coordinated to the TS substrate. A second metal ion is required for cleavage (ball with dash line). It is repelled from the active site by the phosphorothioate modification in DNA. (**F**) Close-up view of the RuvC active site in the locked R-loop state. The coordinated catalytic metal ion (black) is seen contacting the backbone of the incoming NTS DNA. (**G**) Urea-PAGE (polyacrylamide gel electrophoresis) showing time-resolved DNA cleavage. TS is cleaved by HNH prior to NTS cleavage by RuvC, supporting the unlocked/locked R-loop cleavage model. (**H**) Proposed mechanistic model explaining ordered strand cleavage by IscB. (**I**) Small RNA sequencing of purified IscB-RNP, showing partial degradation of the guide RNA and a predictable cleavage site preceding stem-loop P5. (**J**) Domain organization of wild-type and ΔPLMP IscB. (**K**) Urea-PAGE showing time-resolved DNA cleavage by IscB ΔPLMP.8

structure was docked into EM map (Fig. 4, C and D, and fig. S8). Although the HNH core structure agreed with the density very well, manual adjustments were needed to fit the predicted linker structures into the density (fig. S8). The HNH nuclease "bites" onto the sugar-phosphate backbone of TS-DNA in the heteroduplex. The His-rich active site coordinates a catalytic metal ion toward the phosphate of the fourth residue in TS-DNA (Fig. 4E and fig. S9), which would leave 3 nt at the TS-DNA side after cleavage, consistent with the biochemistry (*2*). Topologically, the observed docking movement is only possible if HNH passes underneath NTS-DNA, in a game of limbo with NTS-DNA, which in turn clears the roadblock that previously denied NTS access to RuvC (movie S6). A continuous corridor of density reveals TAM-proximal NTS-DNA entering the RuvC active site, coordinated by a metal ion therein (Fig. 4F and figs. S10 and S11). The order of events explains the biochemical observation that TS-DNA cleavage precedes the NTS cleavage (Fig. 4, G and H). Previously, RuvC in SpCas9 was found to be allosterically controlled by HNH conformational changes (*19*), and its cleavage rate trails behind HNH

(*20*). Our structural analysis defines the structural basis for the allosteric control in IscB (Fig. 4H). The same mechanism is likely present in Cas9 RNP.

Given the robust RNA-guided deoxyribonuclease activity in vitro, it is puzzling to observe only weak genome editing activity from *Ogeu*IscB-ωRNA in human cells (*2*). We noticed the presence of multiple RNA species in the purified *Ogeu*IscB-ωRNA RNP and subjected the sample for RNA deep sequencing. The sequence coverage dropped immediately before the terminator-like P5 element of ωRNA (Fig. 4I). This is rather surprising because P5 density is clearly present in the RNP structure. We speculated that the cryo-EM particle picking and 3D reconstruction process might have inadvertently biased toward P5-containing single particles (fig. S2A). Given the high DNA cleavage activity in our *Ogeu*IscB-ωRNA RNP, we probed into the possibility that the PLMP-P5 interaction may be dispensable for RNA-guided DNA cleavage. Indeed, *Ogeu*IscB-ωRNA with a structure-guided PLMP domain truncation (Δaa1–55) was only slightly slower than the wild-type RNP in target DNA cleavage (Fig. 4, J and K, and fig. S12). This result argues that the PLMP domain is not ubiquitously essential for RNA-guided DNA cleavage among IscB homologs (*2*). We speculate that the PLMP-P5 interaction may instead be important for the biogenesis of IscB-ωRNA, by controlling the readthrough and termination ratio at ωRNA P5 to achieve copy-number balance between IscB and ωRNA. Alternatively, these domains may be important for the transposition of IS200/IS605. The sequencing result further revealed a stepwise decrease in coverage for the guide (after the 6th and 10th nucleotide; Fig. 4I). This pattern is consistent with the observed guide accessibility in the IscB-ωRNA structure (Fig. 1). Whether the guide RNA stability may have been the cause of low genome editing activity in IscB is worth investigation in the future. Indeed, naturally occurring tracrRNA variants containing an 11-nt-long guide were shown to convert *Sp*Cas9 from a nuclease to an RNA-guided transcriptional repressor (*21*). Chemical modification efforts also revealed that the guide RNA integrity could influence the in vivo activity of Cas9 substantially (*22*).

Our structural analysis provides a high-resolution explanation for the relationship between IscB-ωRNA and Cas9-crRNA-tracrRNA. ωRNA was speculated to transpose by itself on the basis of informatic searches (*17*); therefore, it may play more active roles than what the structures revealed. Such functions might no longer be needed, or even be detrimental, when IscB-ωRNA established co-option with the CRISPR system. This may have led to the observed adaptation in Cas9-crRNA-tracrRNA, where the body of ωRNA was entirely replaced by protein domains. The remaining portion serves only two essential functions: guiding RNP assembly and guiding target searching. On the application side, there has been a strong interest to miniaturize Cas9 for expanded usage. For example, it would be desirable to package the next-generation Cas9-based genome editors (*23*–*27*) into mature delivery tools, such as the adenovirus-associated virus (AAV) vectors. Neither structure-guided approach nor directed evolution was particularly successful at miniaturizing the RNA-guided nucleases. By peeking into nature's winning solutions, we gain a fresh starting point to develop a new generation of powerful genome editing tools, packageable into AAV. Fifty-five amino acids have already been removed from IscB without abolishing its activity (Fig. 4I). Further structure-guided efforts will likely lead to smaller, more robust, and more active versions of genome editors.

## REFERENCES AND NOTES


1. V. V. Kapitonov, K. S. Makarova, E. V. Koonin, *J. Bacteriol.* **198**, 797–807 (2015).
2. H. Altae-Tran *et al*., *Science* **374**, 57–65 (2021).
3. T. Karvelis *et al*., *Nature* **599**, 692–696 (2021).
4. M. Jinek *et al*., *Science* **337**, 816–821 (2012).
5. L. Cong *et al*., *Science* **339**, 819–823 (2013).
6. G. Gasiunas, R. Barrangou, P. Horvath, V. Siksnys, *Proc. Natl. Acad. Sci. U.S.A.* **109**, E2579–E2586 (2012).
7. H. Nishimasu *et al*., *Cell* **156**, 935–949 (2014).
8. S. Shmakov *et al*., *Mol. Cell* **60**, 385–397 (2015).
9. F. Jiang *et al*., *Science* **351**, 867–871 (2016).
10. M. Jinek *et al*., *Science* **343**, 1247997 (2014).
11. H. Nishimasu *et al*., *Cell* **162**, 1113–1126 (2015).
12. W. Sun *et al*., *Mol. Cell* **76**, 938–952.e5 (2019).
13. A. Das *et al*., *Nat. Commun.* **11**, 6346 (2020).
14. J. P. K. Bravo *et al*., *Nature* **603**, 343–347 (2022).
15. F. J. M. Mojica, C. Díez-Villaseñor, J. García-Martínez, C. Almendros, *Microbiology (Reading)* **155**, 733–740 (2009).
16. C. Anders, O. Niewoehner, A. Duerst, M. Jinek, *Nature* **513**, 569–573 (2014).
17. Z. Weinberg, J. Perreault, M. M. Meyer, R. R. Breaker, *Nature* **462**, 656–659 (2009).
18. J. Jumper *et al*., *Nature* **596**, 583–589 (2021).
19. S. H. Sternberg, B. LaFrance, M. Kaplan, J. A. Doudna, *Nature* **527**, 110–113 (2015).
20. S. Gong, H. H. Yu, K. A. Johnson, D. W. Taylor, *Cell Rep.* **22**, 359–371 (2018).
21. R. E. Workman *et al*., *Cell* **184**, 675–688.e19 (2021).
22. A. Mir *et al*., *Nat. Commun.* **9**, 2641 (2018).
23. N. M. Gaudelli *et al*., *Nature* **551**, 464–471 (2017).
24. A. V. Anzalone *et al*., *Nature* **576**, 149–157 (2019).
25. A. C. Komor, Y. B. Kim, M. S. Packer, J. A. Zuris, D. R. Liu, *Nature* **533**, 420–424 (2016).
26. A. V. Anzalone *et al*., *Nat. Biotechnol.* **40**, 731–740 (2022).
27. E. I. Ioannidi *et al*., bioRxiv 2021.2011.2001.466786 (2021).


## ACKNOWLEDGMENTS

We thank F. Ding for carrying in vitro RNA transcriptions to test IscB RNP activities, Q. Sun for providing initial IscB Alphafold predictions, and A. Pyle for advice on cryo-EM grid preparation. **Funding:** National Institutes of Health grant GM118174 (A.K.), Department of Defense through the National Defense Science & Engineering Graduate Fellowship Program (G.S.), National Science Foundation Materials Research Science and Engineering Centers program grant DMR-1719875 [Cornell Center for Materials Research Shared DOE Office of Biological and Environmental Research grant KP1607011 (Laboratory for BioMolecular Structure)]. **Author contributions:** Conceptualization: A.K., G.S., C.H.; Methodology: G.S., C.H., A.K. Investigation: G.S., C.H., A.K. Visualization: C.H., G.S., A.K. Funding acquisition: A.K., G.S. Project administration: A.K. Supervision: A.K. Writing – original draft: A.K., G.S., C.H. Writing – review and editing: A.K., G.S., C.H. **Competing interests:** The authors declare competing financial interests on IscB-ωRNA structure-inspired genome editing applications. **Data and materials availability:** The IscB-ωRNA/R-loop coordinates and cryo-EM density map have been deposited in the Protein Data Bank (PDB:7UTN) and the Electron Microscopy Data Bank (EMD-26782). The RNA-sequencing data has been deposited in the Sequence Read Archive (PRJNA838366). Plasmids used in this study are available upon request. 

## SUPPLEMENTARY MATERIALS

science.org/doi/10.1126/science.abq7220
Materials and Methods
Figs. S1 to S12
Table S1
References (*28*)
MDAR Reproducibility Checklist
Movies S1 to S6

View/request a protocol for this paper from *Bio-protocol*.

Submitted 29 April 2022; accepted 18 May 2022
Published online 26 May 2022
10.1126/science.abq7220

# Structural basis for RNA-guided DNA cleavage by IscB-#RNA and mechanistic comparison with Cas9

Gabriel SchulerChunyi HuAilong Ke

*Science*, 376 (6600), • DOI: 10.1126/science.abq7220

**Smaller, simpler, and stealthier**

The evolutionary origin of CRISPR-Cas9 has been traced to the transposon-encoded nuclease IscB. A fraction of the size of Cas9, IscB is just as active as Cas9 in RNA-guided DNA cleavage in test tubes. How did it gradually morph into Cas9? Can we take advantage of its miniature size for expanded genome-editing usage? By solving cryo–electron microscopy structures of IscB-#RNA, Schuler *et al*. provide a high-resolution explanation for IscB's structural and mechanistic similarities to and differences from Cas9. Structure-inspired ideas allowed for the engineering of stealthier versions of IscB and further improvement of IscB's genome-editing activity in human cells. —DJ